

DexYCB: A Benchmark for Capturing Hand Grasping of Objects

Yu-Wei Chao¹ Wei Yang¹ Yu Xiang¹ Pavlo Molchanov¹ Ankur Handa¹ Jonathan Tremblay¹
Yashraj S. Narang¹ Karl Van Wyk¹ Umar Iqbal¹ Stan Birchfield¹ Jan Kautz¹ Dieter Fox^{1,2}

¹NVIDIA, ²University of Washington

{ychao, weiy, yux, pmolchanov, ahanda, jtremblay, ynarang, kvanwyk, uiqbal, sbirchfield, jkautz, dieterf}@nvidia.com



Figure 1: Two captures (left and right) from the DexYCB dataset. In each case, the top row shows color images simultaneously captured from three views, while the bottom row shows the ground-truth 3D object and hand pose rendered on the darkened captured images.

Abstract

We introduce *DexYCB*, a new dataset for capturing hand grasping of objects. We first compare *DexYCB* with a related one through cross-dataset evaluation. We then present a thorough benchmark of state-of-the-art approaches on three relevant tasks: 2D object and keypoint detection, 6D object pose estimation, and 3D hand pose estimation. Finally, we evaluate a new robotics-relevant task: generating safe robot grasps in human-to-robot object handover.¹

1. Introduction

3D object pose estimation and 3D hand pose estimation are two important yet unsolved vision problems. Traditionally, these two problems have been addressed separately, yet in many critical applications, we need both capabilities working together [36, 6, 13]. For example, in robotics, a reliable motion capture for hand manipulation of objects is crucial for both learning from human demonstration [12] and fluent and safe human-robot interaction [46].

State-of-the-art approaches for both 3D object pose [37, 20, 34, 27, 40, 26, 19] and 3D hand pose estimation [49, 23, 18, 2, 9, 14, 31] rely on deep learning and thus require large datasets with labeled hand or object poses for training.

Many datasets [48, 49, 16, 17] have been introduced in both domains and have facilitated progress on these two problems in parallel. However, since they were introduced for either task separately, many of them do not contain interaction of hands and objects, i.e., static objects without humans in the scene, or bare hands without interacting with objects. In the presence of interactions, the challenge of solving the two tasks together not only doubles but multiplies, due to the motion of objects and mutual occlusions incurred by the interaction. Networks trained on either of the datasets will thus not generalize well to interaction scenarios.

Creating a dataset with accurate 3D pose of hands and objects is also challenging for the same reasons. As a result, prior works have attempted to capture accurate hand motion either with specialized gloves [10], magnetic sensors [48, 8], or marker-based mocap systems [3, 35]. While they can achieve unparalleled accuracy, the introduction of hand-attached devices may be intrusive and thus bias the naturalness of hand motion. It also changes the appearance of hands and thus may cause issues with generalization.

Due to the challenge of acquiring real 3D poses, there has been an increasing interest in using synthetic datasets to train pose estimation models. The success has been notable on object pose estimation. Using 3D scanned object models and photorealistic rendering, prior work [16, 34, 38, 5, 17] has generated synthetic scenes of objects with high fidelity in appearance. Their models trained only on synthetic data

¹Dataset and code available at <https://dex-ycb.github.io>.

can thus translate to real images. Nonetheless, synthesizing hand-object interactions remains challenging. One problem is to synthesize realistic grasp poses for generic objects [4]. Furthermore, synthesizing natural looking human motions is still an active research area in graphics.

In this paper, we focus on marker-less data collection of real hand interaction with objects. We take inspiration from recent work [11] and build a multi-camera setup that records interactions synchronously from multiple views. Compared to the recent work, we instrument the setup with more cameras and configure them to capture a larger workspace that allows our human subjects to interact freely with objects. In addition, our pose labeling process utilizes human annotation rather than automatic labeling. We crowdsource the annotation so that we can efficiently scale up the data labeling process. Given the setup, we construct a large-scale dataset that captures a simple yet ubiquitous task: grasping objects from a table. The dataset, DexYCB, consists of 582K RGB-D frames over 1,000 sequences of 10 subjects grasping 20 different objects from 8 views (Fig. 1).

Our contributions are threefold. First, we introduce a new dataset for capturing hand grasping of objects. We empirically demonstrate the strength of our dataset over a related one through cross-dataset evaluation. Second, we provide in-depth analysis of current approaches thoroughly on three relevant tasks: 2D object and keypoint detection, 6D object pose estimation, and 3D hand pose estimation. To the best of our knowledge, our dataset is the first that allows joint evaluation of these three tasks. Finally, we demonstrate the importance of joint hand and object pose estimation on a new robotics relevant task: generating safe robot grasps for human-to-robot object handover.

2. Constructing DexYCB

2.1. Hardware Setup

In order to construct the dataset, we built a multi-camera setup for capturing human hands interacting with objects. A key design choice was to enable a sizable capture space, where a human subject can freely interact and perform tasks with multiple objects. Our multi-camera setup is shown in Fig. 2. We use 8 RGB-D cameras (RealSense D415) and mount them such that collectively they can capture a table-top workspace with minimal blind spots. The cameras are extrinsically calibrated and temporally synchronized. For data collection, we stream and record all 8 views together at 30 fps with both color and depth of resolution 640×480 .

2.2. Data Collection and Annotation

Given the setup, we record videos of hands grasping objects. We use 20 objects from the YCB-Video dataset [44], and record multiple trials from 10 subjects. For each trial, we select a target object with 2 to 4 other objects and place

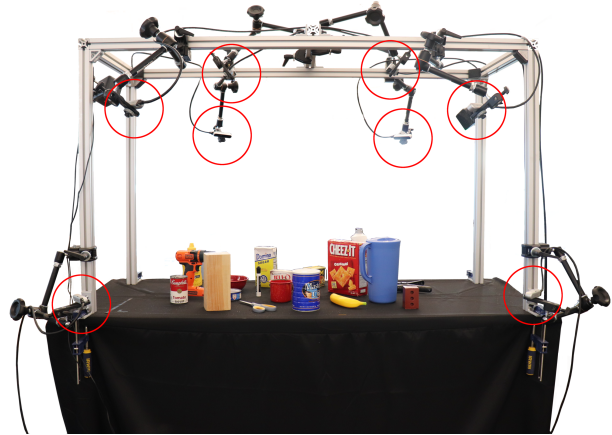


Figure 2: Our setup with 8 RGB-D cameras (red circle).

them on the table. We ask the subject to start from a relaxed pose, pick up the target object, and hold it in the air. We also ask some subjects to pretend to hand over the object to someone across from them. We record for 3 seconds, which is sufficient to contain the full course of action. For each target object, we repeat the trial 5 times, each time with a random set of accompanied objects and placement. We ask the subject to perform the pick-up with the right hand in the first two trials, and with the left hand in the third and fourth trials. In the fifth trial, we randomize the choice. We rotate the target among all 20 objects. This gives us 100 trials per subject, and 1,000 trials in total for all subjects.

To acquire accurate ground-truth 3D pose for hands and objects, our approach (detailed in Sec. 2.3) relies on 2D keypoint annotations for hands and objects in each view. To ensure accuracy, we label the required keypoints in RGB sequences fully through human annotation. Our annotation tool is based on VATIC [39] for efficient annotation of videos. We set up annotation tasks on the Amazon Mechanical Turk (MTurk) and label every view in all the sequences.

For hands, we adopt 21 pre-defined hand joints as our keypoints (3 joints plus 1 tip for each finger and the wrist). We explicitly ask the annotators to label and track these joints throughout a given video sequence. The annotators are also asked to mark a keypoint as invisible in a given frame when it is occluded.

Pre-defining keypoints exhaustively for every object would be laborious and does not scale as the number of objects increases. Our approach (Sec. 2.3) explicitly addresses this issue by allowing user-defined keypoints. Specifically, given a video sequence in a particular view, we first ask the annotator to find 2 distinctive landmark points that are easily identified and trackable on a designated object, and we ask them to label and track these points throughout the sequence. We explicitly ask the annotators to find keypoints that are visible most of the time, and mark a keypoint as invisible whenever it is occluded.

2.3. Solving 3D Hand and Object Pose

To represent 3D hand pose, we use the popular MANO hand model [28]. The model represents a right or left hand with a deformable triangular mesh of 778 vertices. The mesh is parameterized by two low-dimensional embeddings (θ, β) , where $\theta \in \mathbb{R}^{51}$ accounts for variations in pose (i.e. articulation) and $\beta \in \mathbb{R}^{10}$ in shape. We use the version from [14], which implements MANO as a differentiable layer in PyTorch that maps (θ, β) to the mesh together with the 3D positions of 21 hand joints defined in the keypoint annotation. We pre-calibrate the hand shape β for each subject and fix it throughout each subject’s sequences.

Since our objects from YCB-Video [44] also come with texture-mapped 3D mesh models, we use the standard 6D pose representation [16, 17] for 3D object pose. The pose of each object is represented by a matrix $T \in \mathbb{R}^{3 \times 4}$ composed of a 3D rotation matrix and a 3D translation vector.

To solve for hand and object pose, we formulate an optimization problem similar to [50, 11] by leveraging depth and keypoint annotations from all views and multi-view geometry. For a given sequence with N_H hands and N_O objects, we denote the overall pose at a given time frame by $P = (P_H, P_O)$, where $P_H = \{\theta_h\}_{h=1}^{N_H}$ and $P_O = \{T_o\}_{o=1}^{N_O}$. We define the pose in world coordinates where we know the extrinsics of each camera. Then at each time frame, we solve the pose by minimizing the following energy function:

$$E(P) = E_{\text{depth}}(P) + E_{\text{kpt}}(P) + E_{\text{reg}}(P). \quad (1)$$

Depth The depth term E_{depth} measures how well the models given poses explain the observed depth data. Let $\{d_i \in \mathbb{R}^3\}_{i=1}^{N_D}$ be the total point cloud merged from all views after transforming to the world coordinates, with N_D denoting the number of points. Given a pose parameter, we denote the collection of all hand and object meshes as $\mathcal{M}(P) = (\{\mathcal{M}_h(\theta_h)\}, \{\mathcal{M}_o(T_o)\})$. We define the depth term as

$$E_{\text{depth}}(P) = \frac{1}{N_D} \sum_{i=1}^{N_D} |\text{SDF}(d_i, \mathcal{M}(P))|^2, \quad (2)$$

where $\text{SDF}(\cdot)$ calculates the signed distance value of a 3D point from a triangular mesh in mm. While E_{depth} is differentiable, calculating E_{depth} and also the gradients is computationally expensive for large point clouds and meshes with a huge number of vertices. Therefore, we use an efficient point-parallel GPU implementation for it.

Keypoint The keypoint term E_{kpt} measures the reprojection error of the keypoints on the models with the annotated keypoints, and can be decomposed by hand and object:

$$E_{\text{kpt}}(P) = E_{\text{kpt}}(P_H) + E_{\text{kpt}}(P_O). \quad (3)$$

For hands, let $J_{h,j}$ be the 3D position of joint j of hand h in the world coordinates, $p_{h,j}^c$ be the annotation of the

same joint in the image coordinates of view c , and $\gamma_{h,j}^c$ be its visibility indicator. The energy term is defined as

$$E_{\text{kpt}}(P_H) = \frac{1}{\sum \gamma_{h,j}^c} \sum_{c=1}^{N_C} \sum_{h=1}^{N_H} \sum_{j=1}^{N_J} \gamma_{h,j}^c \|\text{proj}^c(J_{h,j}) - p_{h,j}^c\|_2^2, \quad (4)$$

where $\text{proj}^c(\cdot)$ returns the projection of a 3D point onto the image plane of view c , and $N_C = 8$ and $N_J = 21$.

For objects, recall that we did not pre-define keypoints for annotation, but rather asked annotators to select distinctive points to track. Here, we assume an accurate initial pose is given at the first frame where an object’s keypoint is labeled visible. We then map the selected keypoint to a vertex on the object’s 3D model by back-projecting the keypoint’s position onto the object’s visible surface. We fix that mapping afterwards. Let $K_{o,k}^c$ be the 3D position of the selected keypoint k of object o in view c in world coordinates. Similar to Eq. (4), with $N_K = 2$, the energy term is

$$E_{\text{kpt}}(P_O) = \frac{1}{\sum \gamma_{o,k}^c} \sum_{c=1}^{N_C} \sum_{o=1}^{N_O} \sum_{k=1}^{N_K} \gamma_{o,k}^c \|\text{proj}^c(K_{o,k}^c) - p_{o,k}^c\|_2^2. \quad (5)$$

To ensure an accurate initial pose for keypoint mapping, we initialize the pose in each time frame with the solved pose from the last time frame. We initialize the pose in the first frame by running PoseCNN [44] on each view and select an accurate pose for each object manually.

Regularization Following [24, 13], we add an ℓ_2 regularization to the low-dimensional pose embedding of MANO to avoid irregular articulation of hands:

$$E_{\text{reg}}(P) = \frac{1}{N_H} \sum_{h=1}^{N_H} \|\theta_h\|_2^2. \quad (6)$$

To minimize Eq. (1), we use the Adam optimizer with a learning rate of 0.01. For each time frame, we initialize the pose P with the solved pose from the last time frame and run the optimizer for 100 iterations.

3. Related Datasets

3.1. 6D Object Pose

Most datasets address instance-level 6D object pose estimation, where 3D models are given a priori. The recent BOP challenge [16, 17] has curated a decent line-up of these datasets which the participants have to evaluate on. Yet objects are mostly static in these datasets without human interactions. A recent dataset [41] was introduced for category-level 6D pose estimation, but the scenes are also static.

3.2. 3D Hand Pose

We present a summary of related 3D hand pose datasets in Tab. 1. Some address pose estimation with depth only,

| dataset | visual modality | real image | marker-less | hand-hand int | hand-obj int | 3D obj pose | 3D hand shape | resolution | #frames | #sub | #obj | #views | motion | #seq | dynamic grasp | label |
|-------------------------|-----------------|------------|-------------|---------------|--------------|-------------|---------------|------------|---------|------|------|--------|--------|-------|---------------|-----------------------|
| BigHand2.2M [48] | depth | ✓ | × | × | × | – | × | 640×480 | 2,200K | 10 | – | 1 | ✓ | – | – | magnetic sensor |
| SynthHands [25] | RGB-D | × | – | × | ✓ | × | × | 640×480 | 220K | – | 7 | 5 | × | – | – | synthetic |
| Rendered Hand Pose [49] | RGB-D | × | – | × | × | – | × | 320×320 | 44K | 20 | – | 1 | × | – | – | synthetic |
| GANerated Hands [23] | RGB | × | – | × | ✓ | × | × | 256×256 | 331K | – | – | 1 | × | – | – | synthetic |
| ObMan [14] | RGB-D | × | – | × | ✓ | ✓ | ✓ | 256×256 | 154K | 20 | 3K | 1 | × | – | – | synthetic |
| FPHA [8] | RGB-D | ✓ | × | × | ✓ | ✓ | × | 1920×1080 | 105K | 6 | 4 | 1 | ✓ | 1,175 | ✓ | magnetic sensor |
| ContactPose [3] | RGB-D | ✓ | × | × | ✓ | ✓ | ✓ | 960×540 | 2,991K | 50 | 25 | 3 | ✓ | 2,303 | × | mocap + thermal mocap |
| GRAB [35] | – | – | × | × | ✓ | ✓ | ✓ | – | 1,624K | 10 | 51 | – | ✓ | 1,335 | ✓ | mocap |
| Mueller et al. [24] | depth | × | – | ✓ | × | – | × | 640×480 | 80K | 5 | – | 4 | ✓ | 11 | – | synthetic |
| InterHand2.6M [22] | RGB | ✓ | ✓ | ✓ | × | – | ✓ | 512×334 | 2,590K | 27 | – | >80 | ✓ | – | – | semi-auto |
| Dexter+Object [32] | RGB-D | ✓ | ✓ | × | ✓ | ✓ | × | 640×480 | 3K | 2 | 2 | 1 | ✓ | 6 | ✓ | manual |
| Simon et al. [30] | RGB | ✓ | ✓ | × | ✓ | × | × | 1920×1080 | 15K | – | – | 31 | ✓ | – | ✓ | automatic |
| EgoDexter [25] | RGB-D | ✓ | ✓ | × | ✓ | × | × | 640×480 | 3K | 4 | – | 1 | ✓ | 4 | ✓ | manual |
| FreiHAND [50] | RGB | ✓ | ✓ | × | ✓ | × | ✓ | 224×224 | 37K | 32 | 27 | 8 | × | – | – | semi-auto |
| HO-3D [11] | RGB-D | ✓ | ✓ | × | ✓ | ✓ | ✓ | 640×480 | 78K | 10 | 10 | 1–5 | ✓ | 27 | ✓ | automatic |
| DexYCB (ours) | RGB-D | ✓ | ✓ | × | ✓ | ✓ | ✓ | 640×480 | 582K | 10 | 20 | 8 | ✓ | 1,000 | ✓ | manual |

Table 1: Comparison of DexYCB with existing 3D hand pose datasets.

e.g., BigHand2.2M [48]. These datasets can be large but lack color images and capture only bare hands without interactions. Some others address hand-hand interactions, e.g., Mueller et al. [24] and InterHand2.6M [22]. While not focused on interaction with objects, their datasets address another challenging scenario and is orthogonal to our work. Below we review datasets with hand-object interactions.

Synthetic Synthetic data has been increasingly used for hand pose estimation [25, 49, 23, 14]. A common downside is the gap to real images on appearance. To bridge this gap, GANerated Hands [23] was introduced by translating synthetic images to real via GANs. Nonetheless, other challenges remain. One is to synthesize realistic grasp pose for objects. ObMan [14] was introduced to address this challenge using heuristic metrics. Yet besides pose, it is also challenging to synthesize realistic motion. Consequently, these datasets only offer static images but not videos. Our dataset captures real videos with real grasp pose and motion. Furthermore, our motion data from real can help bootstrapping synthetic data generation.

Marker-based FPHA [8] captured hand interaction with objects in first person view by attaching magnetic sensors to the hands. This offers a flexible and portable solution, but the attached sensors may hinder natural hand motion and also bias the hand appearance. ContactPose [3] captured grasp poses by tracking objects with mocap markers and recovering hand pose from thermal imagery of the objects surface. While the dataset is large in scale, the thermal based approach can only capturing rigid grasp poses but not motions. GRAB [35] captured full body motion together with hand-object interactions using marker-based mocap. It provides high-fidelity capture of interactions but does not

come with any visual modalities. Our dataset is marker-less, captures dynamic grasp motions, and provides RGB-D sequences in multiple views.

Marker-less Our DexYCB dataset falls in this category. The challenge is to acquire accurate 3D pose. Some datasets like Dexter+Object [32] and EgoDexter [23] rely on manual annotation and are thus limited in scale. To acquire 3D pose at scale others rely on automatic or semi-automatic approaches [30, 50]. While these datasets capture hand-object interactions, they do not offer 3D pose for objects.

Most similar to ours is the recent HO-3D dataset [11]. HO-3D also captures hands interacting with objects from multiple views and provides both 3D hand and object pose. Nonetheless, the two datasets differ both quantitatively and qualitatively. Quantitatively (Tab. 1), DexYCB captures interactions with more objects (20 versus 10), from more views (8 versus 1 to 5), and is one order of magnitude larger in terms of number of frames (582K versus 78K)² and number of sequences (1,000 versus 27).³ Qualitatively (Fig. 3), we highlight three differences. First, DexYCB captures full grasping processes (i.e. from hand approaching, opening fingers, contact, to holding the object stably) in short segments, whereas HO-3D captures longer sequences with object in hand most of the time. Among the 27 sequences from HO-3D, we found 17 with hand always rigidly attached to the object, only rotating the object from the wrist with no finger articulation. Second, DexYCB captures a full tabletop workspace with 3D pose of all the objects on the table, whereas in HO-3D one object is held close to the camera each time and only the held object is labeled with pose. Finally, regarding annotation, DexYCB leverages keypoints

²We count the number of frames over all views.

³We count the same motion across different views as one sequence.



Figure 3: Qualitative comparison of HO-3D [11] (top) and DexYCB (bottom). DexYCB captures full grasping processes in a tabletop workspace with 3D pose of all the on table objects.

fully labeled by humans through crowdsourcing, while HO-3D relies on a fully automatic labeling pipeline.

4. Cross-Dataset Evaluation

To further assess the merit of our DexYCB dataset, we perform cross-dataset evaluation following prior work [50, 29, 47]. We focus specifically on HO-3D [11] due to its relevance, and evaluate generalizability between HO-3D and DexYCB on single-image 3D hand pose estimation. For DexYCB, we generate a train/val/test split following our benchmark setup (“S0” in Sec. 5.1). For HO-3D, we select 6 out of its 55 training sequences for test. We use Spurr et al. [31] (winner of the HAND 2019 Challenge) as our method, and train the model separately on three training sets: the training set of HO-3D, the training set of DexYCB, and the combined training set from both datasets. Finally, we evaluate the three trained models separately on the test set of HO-3D and DexYCB.

Tab. 2 shows the results in mean per joint position error (MPJPE) reported on two different alignment methods (details in Sec. 5.4). We experiment with two different backbones: ResNet50 and HRNet32 [33]. Unsurprisingly, when training on a single dataset, the model generalizes better to the respective test set. The error increases when tested on the other dataset. When we evaluate the DexYCB trained model on HO-3D, we observe a consistent increase from $1.4\times$ to $1.9\times$ (e.g., for ResNet50, from 18.05 to 31.76 mm on root-relative). However, when we evaluate the HO-3D trained model on DexYCB, we observe a consistent yet more significant increase, from $3.4\times$ to $3.7\times$ (e.g., for ResNet50, from 12.97 to 48.30 mm on root-relative). This suggests that models trained on DexYCB generalize better than on HO-3D. Furthermore, when we train on the combined training set and evaluate on HO-3D, we can further reduce the error from only training on HO-3D (e.g., from 18.05 to 15.79 mm). However, when tested on DexYCB, the error rather rises compared to training only on DexYCB (e.g., from 12.97 to 13.36 mm). We conclude that DexYCB complements HO-3D better than vice versa.

| train \ test | HO-3D [11] | DexYCB | HO-3D [11] + DexYCB |
|--------------|---------------|---------------|---------------------|
| HO-3D | 18.05 / 10.66 | 31.76 / 15.23 | 15.79 / 9.51 |
| DexYCB | 48.30 / 24.23 | 12.97 / 7.18 | 13.36 / 7.27 |
| HO-3D | 17.46 / 10.44 | 33.11 / 15.51 | 15.89 / 9.00 |
| DexYCB | 46.38 / 23.94 | 12.39 / 6.79 | 12.48 / 6.87 |

Table 2: Cross-dataset evaluation with HO-3D [11] on 3D hand pose estimation. Results are in MPJPE (mm) (root-relative / Procrustes aligned). Top: [31] + ResNet50. Bottom: [31] + HRNet32.

5. Benchmarking Representative Approaches

We benchmark three tasks on our DexYCB dataset: 2D object and keypoint detection, 6D object pose estimation, and 3D hand pose estimation. For each task we select representative approaches and analyze their performance.

5.1. Evaluation Setup

To evaluate different scenarios, we generate train/val/test splits in four different ways (referred to as “setup”):

- **S0 (default).** The train split contains all 10 subjects, all 8 camera views, and all 20 grasped objects. Only the sequences are not shared with the val/test split.
- **S1 (unseen subjects).** The dataset is split by subjects (train/val/test: 7/1/2).
- **S2 (unseen views).** The dataset is split by camera views (train/val/test: 6/1/1).
- **S3 (unseen grasping).** The dataset is split by grasped objects (train/val/test: 15/2/3). Objects being grasped in the test split are never being grasped in the train/val split, but may appear static on the table. This way the training set still contain examples of each object.

5.2. 2D Object and Keypoint Detection

We evaluate object and keypoint detection using the COCO evaluation protocol [21]. For object detection, we consider 20 object classes and 1 hand class. We collect ground truths by rendering a segmentation mask for each instance in each camera view. For keypoints, we consider 21 hand joints and collect the ground truths by reprojecting each 3D joint to each camera image.

We benchmark two representative approaches: Mask R-CNN (Detectron2) [15, 43] and SOLOv2 [42]. Mask R-CNN has been the de facto for object and keypoint detection and SOLOv2 is a state-of-the-art on COCO instance segmentation. For both we use a ResNet50-FPN backbone pre-trained on ImageNet and finetune on DexYCB.

Tab. 3 shows results for object detection in average precision (AP). First, Mask R-CNN and SOLOv2 perform similarly in mean average precision (mAP). Mask R-CNN has a slight edge on bounding box (e.g., 75.76 versus 75.13 mAP on S0) while SOLOv2 has a slight edge on segmentation (e.g., 71.56 versus 69.58 mAP on S0). This is because

| | S0 (default) | | | | S1 (unseen subjects) | | | | S2 (unseen views) | | | | S3 (unseen grasping) | | | |
|-----------------------|--------------|--------------|--------------|--------------|----------------------|--------------|--------------|--------------|-------------------|--------------|--------------|--------------|----------------------|--------------|--------------|--------------|
| | Mask R-CNN | | SOLOv2 | | Mask R-CNN | | SOLOv2 | | Mask R-CNN | | SOLOv2 | | Mask R-CNN | | SOLOv2 | |
| | bbox | segm | bbox | segm | bbox | segm | bbox | segm | bbox | segm | bbox | segm | bbox | segm | bbox | segm |
| 002_master_chef_can | 83.87 | 82.68 | 84.90 | 85.20 | 82.41 | 80.69 | 82.74 | 81.67 | 85.82 | 84.44 | 83.52 | 83.39 | 83.96 | 83.72 | 84.53 | 85.44 |
| 003_cracker_box | 85.85 | 83.72 | 89.08 | 88.07 | 82.12 | 80.18 | 84.26 | 84.39 | 88.74 | 87.60 | 89.61 | 87.85 | 85.51 | 83.68 | 79.75 | 88.00 |
| 004_sugar_box | 81.30 | 77.71 | 80.45 | 79.26 | 78.35 | 74.75 | 77.17 | 76.66 | 83.72 | 79.53 | 81.91 | 79.25 | 78.06 | 75.68 | 74.87 | 77.40 |
| 005_tomato_soup_can | 76.03 | 74.75 | 75.70 | 75.33 | 73.65 | 71.33 | 72.66 | 71.35 | 77.66 | 76.70 | 75.25 | 73.82 | 76.70 | 76.29 | 76.50 | 76.48 |
| 006_mustard_bottle | 81.56 | 79.40 | 79.94 | 81.87 | 78.76 | 75.41 | 77.76 | 75.92 | 81.12 | 79.06 | 79.87 | 78.29 | 81.74 | 82.37 | 82.24 | 84.45 |
| 007_tuna_fish_can | 68.08 | 67.14 | 67.76 | 67.34 | 68.99 | 67.76 | 68.07 | 67.59 | 73.37 | 72.06 | 71.72 | 70.68 | 75.76 | 77.70 | 75.76 | 77.61 |
| 008_pudding_box | 73.60 | 70.39 | 74.05 | 72.58 | 69.77 | 68.04 | 69.78 | 68.20 | 78.88 | 76.74 | 79.01 | 76.58 | 71.32 | 71.43 | 65.11 | 70.94 |
| 009_gelatin_box | 69.51 | 68.43 | 68.64 | 68.09 | 67.37 | 64.99 | 66.16 | 63.14 | 72.87 | 71.45 | 73.34 | 69.36 | 61.19 | 58.41 | 60.98 | 59.49 |
| 010_potted_meat_can | 75.63 | 72.66 | 77.28 | 75.80 | 73.86 | 71.95 | 70.87 | 71.76 | 78.96 | 78.35 | 79.63 | 76.84 | 77.48 | 78.03 | 78.40 | 79.24 |
| 011_banana | 70.53 | 63.43 | 69.67 | 65.49 | 68.07 | 60.50 | 67.31 | 60.57 | 72.46 | 58.18 | 70.80 | 70.68 | 71.67 | 67.54 | 73.25 | 70.28 |
| 019_pitcher_base | 87.17 | 84.67 | 89.95 | 88.98 | 86.21 | 82.00 | 90.07 | 86.38 | 90.47 | 86.67 | 86.88 | 87.02 | 85.62 | 83.69 | 90.22 | 89.91 |
| 021_bleach_cleanser | 80.98 | 77.52 | 75.52 | 79.71 | 79.59 | 76.68 | 78.77 | 78.52 | 84.75 | 81.71 | 82.79 | 81.75 | 77.36 | 71.54 | 77.01 | 75.54 |
| 024_bowl | 80.62 | 78.12 | 75.79 | 80.30 | 78.75 | 76.42 | 78.06 | 77.39 | 83.25 | 80.12 | 81.54 | 79.72 | 81.12 | 79.69 | 81.91 | 82.99 |
| 025_mug | 76.01 | 71.95 | 76.35 | 74.35 | 74.64 | 69.64 | 72.72 | 69.93 | 80.14 | 75.99 | 78.24 | 74.13 | 75.51 | 73.19 | 76.78 | 75.86 |
| 035_power_drill | 81.83 | 73.80 | 82.85 | 77.20 | 76.89 | 69.02 | 77.90 | 71.50 | 82.57 | 74.66 | 82.42 | 74.09 | 83.67 | 77.62 | 84.06 | 80.77 |
| 036_wood_block | 83.75 | 81.41 | 85.72 | 85.59 | 80.45 | 78.15 | 79.45 | 79.32 | 83.78 | 83.40 | 41.24 | 64.85 | 77.52 | 73.84 | 78.01 | 77.78 |
| 037_scissors | 64.07 | 29.36 | 59.00 | 32.63 | 55.05 | 20.68 | 50.85 | 26.51 | 63.16 | 17.93 | 38.00 | 16.93 | 58.01 | 24.35 | 57.92 | 31.11 |
| 040_large_marker | 52.69 | 42.42 | 50.95 | 42.46 | 50.14 | 38.46 | 44.94 | 36.46 | 53.98 | 36.47 | 50.78 | 33.58 | 55.35 | 41.23 | 53.66 | 45.22 |
| 052_extra_large_clamp | 73.41 | 54.03 | 71.71 | 55.38 | 68.12 | 51.26 | 65.26 | 52.33 | 75.61 | 52.77 | 61.14 | 53.59 | 75.24 | 57.28 | 72.52 | 58.87 |
| 061_foam_brick | 72.68 | 72.85 | 72.54 | 72.93 | 68.34 | 66.62 | 67.98 | 65.72 | 75.24 | 74.10 | 73.01 | 71.05 | 71.36 | 71.32 | 71.50 | 71.59 |
| hand | 71.85 | 54.83 | 66.41 | 54.27 | 64.88 | 46.86 | 58.33 | 46.66 | 70.23 | 54.70 | 59.28 | 52.08 | 71.23 | 54.89 | 66.33 | 53.51 |
| mAP | 75.76 | 69.58 | 75.13 | 71.56 | 72.69 | 66.26 | 71.48 | 67.24 | 77.94 | 70.60 | 72.37 | 68.66 | 75.02 | 69.69 | 74.35 | 72.05 |

Table 3: 2D object detection results in AP (%) on the four setups. We compare Mask R-CNN (Detectron2) [15, 43] with SOLOv2 [42] on both bounding box (bbox) and segmentation (segm).

| | S0 | S1 | S2 | S3 |
|------|-------|-------|-------|-------|
| hand | 36.42 | 26.85 | 32.90 | 35.18 |

Table 4: 2D keypoint detection results in AP (%) with Mask R-CNN (Detectron2) [15, 43].

Mask R-CNN predicts bounding boxes first and uses them to generate segmentations. Therefore the error can accumulate for segmentation. SOLOv2 in contrast directly predicts segmentations and uses it to generate bounding boxes. Second, the AP for hand is lower than the AP for objects (e.g., for Mask R-CNN, 71.85 for hand versus 75.76 mAP on S0 bbox). This suggests that hands are more difficult to detect than objects, possibly due to its larger variability in position. Finally, performance varies across setups. For example, mAP in S1 is lower than in S0 (e.g., for Mask R-CNN, 72.69 versus 75.76 on bbox). This can be attributed to the challenge introduced by unseen subjects. Tab. 4 shows the AP for keypoint detection with Mask R-CNN. We observe a similar trend on the ordering of AP over different setups.

5.3. 6D Object Pose Estimation

We evaluate single-view 6D pose estimation following the BOP challenge protocol [16, 17]. The task asks for a 6D pose estimate for each object instance given the number of objects and instances in each image. The evaluation computes recall using three different pose-error functions (VSD, MSSD, MSPD), and the final score is the average of the three recall values (AR).

We first analyze the challenge brought by hand grasping by comparing static and grasped objects. We use PoseCNN

| all | static | grasped |
|-------|--------|---------|
| 52.68 | 56.53 | 41.65 |

Table 5: PoseCNN (RGB) [44] results in AR (%) on S0 (default).

(RGB) [44] as a baseline and retrain the model on DexYCB. Tab. 5 shows the AR on S0 evaluated separately on the full test set, static objects only, and grasped objects only. Without surprise the AR drops significantly when only considering the grasped objects. This recapitulates the increasing challenge of object pose estimation under hand interactions. To better focus on this regime, we evaluate only on the grasped objects in the remaining experiments.

We next evaluate on the four setups using the same baseline. Results are shown in Tab. 6 (left). On S1 (unseen subjects), we observe a drop in AR compared to S0 (e.g., 38.26 versus 41.65 on all) as in object detection. This can be attributed to the influence of interaction from unseen hands as well as different grasping styles. The column of S3 (unseen grasping) shows the AR of the three only objects being grasped in the test set (i.e. “009_gelatin_box”, “021_bleach_cleanser”, “036_wood_block”). Again, the AR is lower compared to on S0, and the drop is especially significant for smaller objects like “009_gelatin_box” (33.07 versus 46.62). Surprisingly, AR on S2 (unseen views) does not drop but rather increases slightly (e.g., 45.18 versus 41.65 on all). This suggests that our multi-camera setup has a dense enough coverage of the scene such that training on certain views can translate well to some others.

Finally, we benchmark five representative approaches: PoseCNN [44], DeepIM [20], DOPE [38], PoseRBPF [5],

| | S0 | S1 | S2 | S3 | PoseCNN [44] | | DeepIM [20] | | DOPE [38] | PoseRBPF [5] | | CosyPose [19] |
|-----------------------|-------|-------|-------|-------|--------------|-------------|-------------|--------------|-----------|--------------|--------------|---------------|
| | | | | | RGB | + depth ref | RGB | RGB-D | RGB | RGB | RGB-D | RGB |
| 002_master_chef_can | 47.47 | 44.53 | 51.36 | – | 44.53 | 48.24 | 60.74 | 68.40 | 19.82 | 35.19 | 58.04 | 77.21 |
| 003_cracker_box | 61.04 | 57.46 | 60.65 | – | 57.46 | 62.62 | 79.43 | 84.56 | 53.50 | 43.62 | 67.37 | 88.39 |
| 004_sugar_box | 45.11 | 36.00 | 51.73 | – | 36.00 | 42.45 | 51.29 | 59.34 | 32.06 | 30.55 | 56.55 | 69.61 |
| 005_tomato_soup_can | 36.68 | 34.88 | 45.44 | – | 34.88 | 42.99 | 46.87 | 55.46 | 20.52 | 23.76 | 40.03 | 52.76 |
| 006_mustard_bottle | 52.56 | 42.89 | 51.96 | – | 42.89 | 48.98 | 55.52 | 63.31 | 23.66 | 28.98 | 54.93 | 67.11 |
| 007_tuna_fish_can | 32.70 | 29.58 | 31.96 | – | 29.58 | 36.17 | 39.18 | 46.98 | 5.86 | 20.13 | 36.77 | 49.00 |
| 008_pudding_box | 44.24 | 42.60 | 50.81 | – | 42.60 | 51.26 | 58.23 | 67.18 | 14.48 | 27.24 | 47.95 | 70.22 |
| 009_gelatin_box | 46.62 | 34.39 | 44.38 | 33.07 | 34.39 | 41.71 | 47.89 | 55.54 | 21.81 | 31.27 | 46.14 | 57.63 |
| 010_potted_meat_can | 37.41 | 42.10 | 45.08 | – | 42.10 | 51.64 | 60.19 | 69.40 | 14.15 | 31.17 | 46.43 | 65.37 |
| 011_banana | 38.33 | 36.71 | 44.42 | – | 36.71 | 40.21 | 41.82 | 48.63 | 16.15 | 21.39 | 39.15 | 35.48 |
| 019_pitcher_base | 53.49 | 46.03 | 53.51 | – | 46.03 | 49.62 | 54.27 | 63.46 | 7.02 | 19.94 | 51.38 | 52.68 |
| 021_bleach_cleanser | 49.41 | 42.54 | 56.03 | 38.52 | 42.54 | 46.29 | 51.54 | 61.44 | 16.70 | 22.94 | 53.50 | 63.62 |
| 024_bowl | 57.42 | 54.25 | 58.15 | – | 54.25 | 57.05 | 60.30 | 69.40 | – | 37.00 | 62.49 | 74.74 |
| 025_mug | 40.68 | 37.28 | 43.70 | – | 37.28 | 38.69 | 41.15 | 49.51 | – | 18.21 | 34.87 | 48.48 |
| 035_power_drill | 47.93 | 41.86 | 50.79 | – | 41.86 | 45.79 | 58.10 | 64.28 | 19.60 | 30.67 | 51.41 | 49.22 |
| 036_wood_block | 40.11 | 38.66 | 49.50 | 40.53 | 38.66 | 44.08 | 49.91 | 65.39 | – | 23.80 | 51.63 | 67.14 |
| 037_scissors | 21.93 | 22.87 | 25.90 | – | 22.87 | 25.29 | 27.48 | 32.65 | 14.16 | 17.18 | 29.40 | 24.36 |
| 040_large_marker | 35.09 | 32.12 | 38.19 | – | 32.12 | 38.73 | 33.27 | 46.63 | – | 19.05 | 29.66 | 50.58 |
| 052_extra_large_clamp | 30.48 | 31.89 | 34.42 | – | 31.89 | 33.60 | 39.63 | 47.04 | – | 22.99 | 35.99 | 50.78 |
| 061_foam_brick | 12.80 | 13.04 | 15.75 | – | 13.04 | 16.70 | 18.14 | 27.57 | – | 17.40 | 32.42 | 30.12 |
| all | 41.65 | 38.26 | 45.18 | 37.41 | 38.26 | 43.27 | 48.99 | 57.54 | – | 26.24 | 46.48 | 57.43 |

Table 6: 6D object pose estimation results in AR (%). Left: PoseCNN (RGB). Right: performance of representative approaches on S1.

and CosyPose [19] (winner of the BOP challenge 2020). All of them take RGB input. For PoseCNN, we also include a variant with post-process depth refinement. For DeepIM and PoseRBPF, we also include their RGB-D variants. For CosyPose, we use its single view version. For DeepIM and CosyPose, we initialize the pose from the output of PoseCNN (RGB). We retrain all the models on DexYCB except for DOPE and PoseRBPF, which trained their models solely on synthetic images. For DOPE, we train models for an additional 7 objects besides the 5 provided. Tab. 6 (right) compares the results on the most challenging S1 (unseen subjects) setup. First, we can see a clear edge on those which also use depth compared to their respective RGB only variants (for PoseCNN, from 38.26 to 43.27 AR on all). Second, refinement based methods like DeepIM and CosyPose are able to improve significantly upon their initial pose input (e.g., for DeepIM RGB-D, from 38.26 to 57.54 AR on all). Finally, CosyPose achieves the best overall AR among all the RGB-based methods (57.43 AR on all).

5.4. 3D Hand Pose Estimation

The task is to estimate the 3D position of 21 hand joints from a single image. We evaluate with two metrics: mean per joint position error (MPJPE) in mm and percentage of correct keypoints (PCK). Besides computing error in absolute 3D position, we also report errors after aligning the predictions with ground truths in post-processing [49, 50, 11]. We consider two alignment methods: root-relative and Procrustes. The former removes ambiguity in translation by replacing the root (wrist) location with ground truths. The latter removes ambiguity in translation, rotation, and scale, thus focusing specifically on articulation. For PCK we re-

| | | absolute | root-relative | Procrustes |
|----|-----------------|----------------------|----------------------|---------------------|
| S0 | [31] + ResNet50 | 53.92 (0.307) | 17.71 (0.683) | 7.12 (0.858) |
| | [31] + HRNet32 | 52.26 (0.328) | 17.34 (0.698) | 6.83 (0.864) |
| | A2J [45] | 27.53 (0.612) | 23.93 (0.588) | 12.07 (0.760) |
| S1 | [31] + ResNet50 | 70.23 (0.240) | 22.71 (0.601) | 8.43 (0.832) |
| | [31] + HRNet32 | 70.10 (0.248) | 22.26 (0.615) | 7.98 (0.841) |
| | A2J [45] | 29.09 (0.584) | 25.57 (0.562) | 12.95 (0.743) |
| S2 | [31] + ResNet50 | 83.46 (0.208) | 23.15 (0.566) | 8.11 (0.838) |
| | [31] + HRNet32 | 80.63 (0.217) | 25.49 (0.530) | 8.21 (0.836) |
| | A2J [45] | 23.44 (0.576) | 27.65 (0.540) | 13.42 (0.733) |
| S3 | [31] + ResNet50 | 58.69 (0.281) | 19.41 (0.665) | 7.56 (0.849) |
| | [31] + HRNet32 | 55.39 (0.311) | 18.44 (0.686) | 7.06 (0.859) |
| | A2J [45] | 30.99 (0.608) | 24.92 (0.581) | 12.15 (0.759) |

Table 7: 3D hand pose estimation results in MPJPE (mm). Numbers in parentheses are AUC values.

port the area under the curve (AUC) over the error range [0, 50 mm] with 100 steps.

We benchmark one RGB and one depth based approach. For RGB, we select a supervised version of Spurr et al. [31] which won the HANDS 2019 Challenge [1]. We experiment with the original ResNet50 backbone as well as a stronger HRNet32 [33] backbone, both initialized with ImageNet pre-trained models and finetuned on DexYCB. For depth, we select A2J [45] and retrain the model on DexYCB.

Tab. 7 shows the results. For [31], we can see that estimating absolute 3D position solely from RGB is difficult (e.g., 53.92 mm absolute MPJPE with ResNet50 on S0). The stronger HRNet32 backbone reduces the errors over ResNet50 but only marginally (e.g., 52.26 versus 53.92 mm absolute MPJPE on S0). Similar to in object pose, the errors on S1 (unseen subjects) increase from S0 (e.g., 70.10 versus 52.26 mm absolute MPJPE for HRNet32) due to the impact of unseen hands and grasping styles. However, unlike the trend in Tab. 6 (left), the errors on S2 (unseen views) also in-

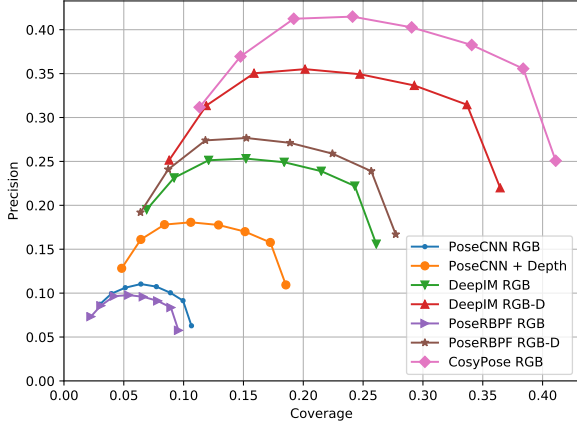


Figure 4: Precision-coverage curves for grasp generation on S1.

crease pronouncedly and even surpass the other setups (e.g., 80.63 mm absolute MPJPE for HRNet32). This is because unlike objects, the subjects are always facing the same direction from a situated position in this setup. This further constrains the possible hand poses observed in each view, making cross view generalization more challenging. Unsurprisingly, A2J [45] outperforms [31] on absolute MPJPE due to the depth input, but falls short on estimating articulation as shown by the errors after alignment (e.g., 12.07 versus 6.83 mm Procrustes MPJPE for HRNet32 on S0).

6. Safe Human-to-Robot Object Handover

Task Given an RGB-D image with a person holding an object, the goal is to generate a diverse set of robot grasps to take over the object without pinching the person’s hand (we refer to as “safe” handovers). The diversity of grasps is important since not all the grasps are kinematically feasible for execution. We assume a parallel-jaw Franka Panda gripper and represent each grasp as a point in $SE(3)$.

Evaluation We first sample 100 grasps for each YCB object using farthest point sampling from a diverse set of grasps pre-generated for that object in [7]. This ensures a dense coverage of the pose space (Fig. 5). For each image, we transform these grasps from the object frame to camera frame using the ground-truth object pose, and remove those collided with the ground-truth object and hand mesh. This generates a reference set of successful grasps \mathcal{R} .

Given a set of predicted grasps χ , we evaluate its diversity by computing the *coverage* [7] of \mathcal{R} , defined by the percentage of grasps in \mathcal{R} having at least one matched grasp in χ that is neither collided with the object nor the hand. Specifically, two grasps g, h are considered matched if $|g_t - h_t| < \sigma_t$ and $\arccos(|\langle g_q, h_q \rangle|) < \sigma_q$, where g_t is the translation and g_q is the orientation in quaternion. We use $\sigma_t = 0.05$ m and $\sigma_q = 15^\circ$.

One could potentially hit a high coverage by sampling grasps exhaustively. Therefore we also compute *precision*,

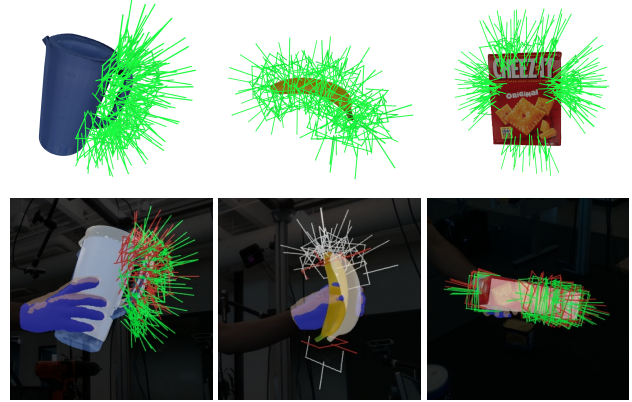


Figure 5: Top: 100 successful grasps sampled from [7]. Bottom: predicted grasps generated by the predicted object pose (textured model) and hand segmentation (blue masks). Green ones denote those covering successful grasps, red ones denote those collided with the object or hand, and gray ones are failures not covering any successful grasps in the reference set. Ground-truth objects and hands are shown in translucent white and brown meshes.

defined as the percentage of grasps in χ that have at least one matched successful grasp in \mathcal{R} .

Baseline We experiment with a simple baseline that only requires hand segmentation and 6D object pose. Similar to constructing \mathcal{R} , we transform the 100 grasps to the camera frame but using the estimated object pose, then remove those that are collided with the hand point cloud obtained by the hand segmentation and the depth image. Specifically, a grasp is collided if the distance of a pair of points from the gripper point cloud and the hand point cloud is less than a threshold ϵ . The gripper point cloud is obtained from a set of pre-sampled points on the gripper surface. We use the hand segmentation results from Mask R-CNN (Sec. 5.2).

Results We evaluate grasps generated with different object pose methods at different threshold $\epsilon \in [0, 0.07$ m] and show the precision-coverage curves on S1 in Fig. 4. We see that better object pose estimation leads to better grasp generation. Fig. 5 shows qualitative examples of the predicted grasps. We see that most of the failure grasps (red and gray) are due to inaccurate object pose. Some are hand-colliding grasps caused by a miss detected hand when the hand is partially occluded by the object (e.g., “003_cracker_box”). This can be potentially addressed by model based approaches that directly predict the full hand shape.

7. Conclusions

We have introduced DexYCB for capturing hand grasping of objects. We have shown its merits, presented a thorough benchmark of current approaches on three relevant tasks, and evaluated a new robotics-relevant task. We envision our dataset will drive progress on these crucial fronts.

References

- [1] Anil Armagan, Guillermo Garcia-Hernando, Seungryul Baek, Shreyas Hampali, Mahdi Rad, Zhaohui Zhang, Shipeng Xie, Mingxiu Chen, Boshen Zhang, Fu Xiong, Yang Xiao, Zhiguo Cao, Junsong Yuan, Pengfei Ren, Weiting Huang, Haifeng Sun, Marek Hruz, Jakub Kanis, Zdeněk Krňoul, Qingfu Wan, Shile Li, Linlin Yang, Dongheui Lee, Angela Yao, Weiguo Zhou, Sijia Mei, Yunhui Liu, Adrian Spurr, Umar Iqbal, Pavlo Molchanov, Philippe Weinzaepfel, Romain Brégier, Grégory Rogez, Vincent Lepetit, and Tae-Kyun Kim. Measuring generalisation to unseen viewpoints, articulations, shapes and objects for 3D hand pose estimation under hand-object interaction. In *ECCV*, 2020. 7
- [2] Adnane Boukhayma, Rodrigo de Bem, and Philip H.S. Torr. 3D hand shape and pose from images in the wild. In *CVPR*, 2019. 1
- [3] Samarth Brahmabhatt, Chengcheng Tang, Christopher D. Twigg, Charles C. Kemp, and James Hays. ContactPose: A dataset of grasps with object contact and hand pose. In *ECCV*, 2020. 1, 4
- [4] Enric Corona, Albert Pumarola, Guillem Alenyà, Francesc Moreno-Noguer, and Grégory Rogez. GanHand: Predicting human grasp affordances in multi-object scenes. In *CVPR*, 2020. 2
- [5] Xinke Deng, Arsalan Mousavian, Yu Xiang, Fei Xia, Timothy Bretl, and Dieter Fox. PoseRBPF: A Rao-Blackwellized particle filter for 6D object pose estimation. In *RSS*, 2019. 1, 6, 7
- [6] Bardia Doosti, Shujon Naha, Majid Mirbagheri, and David J. Crandall. HOPE-Net: A graph-based model for hand-object pose estimation. In *CVPR*, 2020. 1
- [7] Clemens Eppner, Arsalan Mousavian, and Dieter Fox. A billion ways to grasps: An evaluation of grasp sampling schemes on a dense, physics-based grasp data set. In *ISRR*, 2019. 8
- [8] Guillermo Garcia-Hernando, Shanxin Yuan, Seungryul Baek, and Tae-Kyun Kim. First-person hand action benchmark with RGB-D videos and 3D hand pose annotations. In *CVPR*, 2018. 1, 4
- [9] Lihao Ge, Zhou Ren, Yuncheng Li, Zehao Xue, Yingying Wang, Jianfei Cai, and Junsong Yuan. 3D hand shape and pose estimation from a single RGB image. In *CVPR*, 2019. 1
- [10] Oliver Glauser, Shihao Wu, Daniele Panozzo, Otmar Hilliges, and Olga Sorkine-Hornung. Interactive hand pose estimation using a stretch-sensing soft glove. In *SIGGRAPH*, 2019. 1
- [11] Shreyas Hampali, Mahdi Rad, Markus Oberweger, and Vincent Lepetit. HONotate: A method for 3D annotation of hand and object poses. In *CVPR*, 2020. 2, 3, 4, 5, 7
- [12] Ankur Handa, Karl Van Wyk, Wei Yang, Jacky Liang, Yu-Wei Chao, Qian Wan, Stan Birchfield, Nathan Ratliff, and Dieter Fox. DexPilot: Vision-based teleoperation of dexterous robotic hand-arm system. In *ICRA*, 2020. 1
- [13] Yana Hasson, Bugra Tekin, Federica Bogo, Ivan Laptev, Marc Pollefeys, and Cordelia Schmid. Leveraging photometric consistency over time for sparsely supervised hand-object reconstruction. In *CVPR*, 2020. 1, 3
- [14] Yana Hasson, Gul Varol, Dimitrios Tzionas, Igor Kalevatykh, Michael J. Black, Ivan Laptev, and Cordelia Schmid. Learning joint reconstruction of hands and manipulated objects. In *CVPR*, 2019. 1, 3, 4
- [15] Kaiming He, Georgia Gkioxari, Piotr Dollár, and Ross Girshick. Mask R-CNN. In *ICCV*, 2017. 5, 6
- [16] Tomáš Hodaň, Frank Michel, Eric Brachmann, Wadim Kehl, Anders Glent Buch, Dirk Kraft, Bertram Drost, Joel Vidal, Stephan Ihrke, Xenophon Zabulis, Caner Sahin, Fabian Manhardt, Federico Tombari, Tae-Kyun Kim, Jiří Matas, and Carsten Rother. BOP: Benchmark for 6D object pose estimation. In *ECCV*, 2018. 1, 3, 6
- [17] Tomáš Hodaň, Martin Sundermeyer, Bertram Drost, Yann Labbé, Eric Brachmann, Frank Michel, Carsten Rother, and Jiří Matas. BOP challenge 2020 on 6D object localization. *ECCV Workshops*, 2020. 1, 3, 6
- [18] Umar Iqbal, Pavlo Molchanov, Thomas Breuel, Juergen Gall, and Jan Kautz. Hand pose estimation via latent 2.5D heatmap regression. In *ECCV*, 2018. 1
- [19] Yann Labbé, Justin Carpentier, Mathieu Aubry, and Josef Sivic. CosyPose: Consistent multi-view multi-object 6D pose estimation. In *ECCV*, 2020. 1, 7
- [20] Yi Li, Gu Wang, Xiangyang Ji, Yu Xiang, and Dieter Fox. DeepIM: Deep iterative matching for 6D pose estimation. In *ECCV*, 2018. 1, 6, 7
- [21] Tsung-Yi Lin, Michael Maire, Serge Belongie, James Hays, Pietro Perona, Deva Ramanan, Piotr Dollár, and C. Lawrence Zitnick. Microsoft COCO: Common objects in context. In *ECCV*, 2014. 5
- [22] Gyeongsik Moon, Shou-I Yu, He Wen, Takaaki Shiratori, and Kyoung Mu Lee. InterHand2.6M: A dataset and baseline for 3D interacting hand pose estimation from a single RGB image. In *ECCV*, 2020. 4
- [23] Franziska Mueller, Florian Bernard, Oleksandr Sotnychenko, Dushyant Mehta, Srinath Sridhar, Dan Casas, and Christian Theobalt. GANerated Hands for real-time 3D hand tracking from monocular RGB. In *CVPR*, 2018. 1, 4
- [24] Franziska Mueller, Micah Davis, Florian Bernard, Oleksandr Sotnychenko, Mickeal Verschoor, Miguel A. Otaduy, Dan Casas, and Christian Theobalt. Real-time pose and shape reconstruction of two interacting hands with a single depth camera. In *SIGGRAPH*, 2019. 3, 4
- [25] Franziska Mueller, Dushyant Mehta, Oleksandr Sotnychenko, Srinath Sridhar, Dan Casas, and Christian Theobalt. Real-time hand tracking under occlusion from an egocentric RGB-D sensor. In *ICCV*, 2017. 4
- [26] Kiru Park, Timothy Patten, and Markus Vincze. Pix2Pose: Pixel-wise coordinate regression of objects for 6D pose estimation. In *ICCV*, 2019. 1
- [27] Sida Peng, Yuan Liu, Qixing Huang, Xiaowei Zhou, and Hujun Bao. PVNet: Pixel-wise voting network for 6DoF pose estimation. In *CVPR*, 2019. 1
- [28] Javier Romero, Dimitrios Tzionas, and Michael J. Black. Embodied hands: Modeling and capturing hands and bodies together. In *SIGGRAPH Asia*, 2017. 3

- [29] Dandan Shan, Jiaqi Geng, Michelle Shu, and David F. Fouhey. Understanding human hands in contact at internet scale. In *CVPR*, 2020. 5
- [30] Tomas Simon, Hanbyul Joo, Iain Matthews, and Yaser Sheikh. Hand keypoint detection in single images using multiview bootstrapping. In *CVPR*, 2017. 4
- [31] Adrian Spurr, Umar Iqbal, Pavlo Molchanov, Otmar Hilliges, and Jan Kautz. Weakly supervised 3D hand pose estimation via biomechanical constraints. In *ECCV*, 2020. 1, 5, 7, 8
- [32] Srinath Sridhar, Franziska Mueller, Michael Zollhoefer, Dan Casas, Antti Oulasvirta, and Christian Theobalt. Real-time joint tracking of a hand manipulating an object from RGB-D input. In *ECCV*, 2016. 4
- [33] Ke Sun, Bin Xiao, Dong Liu, and Jingdong Wang. Deep high-resolution representation learning for human pose estimation. In *CVPR*, 2019. 5, 7
- [34] Martin Sundermeyer, Zoltan-Csaba Marton, Maximilian Durner, Manuel Brucker, and Rudolph Triebel. Implicit 3D orientation learning for 6D object detection from RGB images. In *ECCV*, 2018. 1
- [35] Omid Taheri, Nima Ghorbani, Michael J. Black, and Dimitrios Tzionas. GRAB: A dataset of whole-body human grasping of objects. In *ECCV*, 2020. 1, 4
- [36] Bugra Tekin, Federica Bogo, and Marc Pollefeys. H+O: Unified egocentric recognition of 3D hand-object poses and interactions. In *CVPR*, 2019. 1
- [37] Bugra Tekin, Sudipta N. Sinha, and Pascal Fua. Real-time seamless single shot 6D object pose prediction. In *CVPR*, 2018. 1
- [38] Jonathan Tremblay, Thang To, Balakumar Sundaralingam, Yu Xiang, Dieter Fox, and Stan Birchfield. Deep object pose estimation for semantic robotic grasping of household objects. In *CoRL*, 2018. 1, 6, 7
- [39] Carl Vondrick, Donald Patterson, and Deva Ramanan. Efficiently scaling up crowdsourced video annotation. *IJCV*, 101(1):184–204, Jan 2013. 2
- [40] Chen Wang, Danfei Xu, Yuke Zhu, Roberto Martin-Martin, Cewu Lu, Li Fei-Fei, and Silvio Savarese. DenseFusion: 6D object pose estimation by iterative dense fusion. In *CVPR*, 2019. 1
- [41] He Wang, Srinath Sridhar, Jingwei Huang, Julien Valentin, Shuran Song, and Leonidas J. Guibas. Normalized object coordinate space for category-level 6D object pose and size estimation. In *CVPR*, 2019. 3
- [42] Xinlong Wang, Rufeng Zhang, Tao Kong, Lei Li, and Chunhua Shen. SOLOv2: Dynamic, faster and stronger. In *NeurIPS*. 2020. 5, 6
- [43] Yuxin Wu, Alexander Kirillov, Francisco Massa, Wan-Yen Lo, and Ross Girshick. Detectron2. <https://github.com/facebookresearch/detectron2>, 2019. 5, 6
- [44] Yu Xiang, Tanner Schmidt, Venkatraman Nafurayanan, and Dieter Fox. PoseCNN: A convolutional neural network for 6D object pose estimation in cluttered scenes. In *RSS*, 2018. 2, 3, 6, 7
- [45] Fu Xiong, Boshen Zhang, Yang Xiao, Zhiguo Cao, Taidong Yu, Joey Tianyi Zhou, and Junsong Yuan. A2J: Anchor-to-joint regression network for 3D articulated pose estimation from a single depth image. In *ICCV*, 2019. 7, 8
- [46] Wei Yang, Chris Paxton, Maya Cakmak, and Dieter Fox. Human grasp classification for reactive human-to-robot handovers. In *IROS*, 2020. 1
- [47] Zhixuan Yu, Jae Shin Yoon, In Kyu Lee, Prashanth Venkatesh, Jaesik Park, Jihun Yu, and Hyun Soo Park. HUMBI: A large multiview dataset of human body expressions. In *CVPR*, 2020. 5
- [48] Shanxin Yuan, Qi Ye, Bjorn Stenger, Siddhant Jain, and Tae-Kyun Kim. BigHand2.2M benchmark: Hand pose dataset and state of the art analysis. In *CVPR*, 2017. 1, 4
- [49] Christian Zimmermann and Thomas Brox. Learning to estimate 3D hand pose from single RGB images. In *ICCV*, 2017. 1, 4, 7
- [50] Christian Zimmermann, Duygu Ceylan, Jimei Yang, Bryan Russell, Max J. Argus, and Thomas Brox. FreiHAND: A dataset for markerless capture of hand pose and shape from single RGB images. In *ICCV*, 2019. 3, 4, 5, 7